Solidification Behavior of the Benzamide + *O*-Chlorobenzoic Acid Eutectic System†

Nakshatra Bahadur Singh, Tanvi Agrawal, Preeti Gupta, and Shiva Saran Das*

Department of Chemistry, DDU Gorakhpur University, Gorakhpur-273009, India

The phase diagram of the benzamide + *o*-chlorobenzoic acid system has been studied by the thaw−melt method, and results show the formation of a simple eutectic mixture. Values of enthalpies of fusion of pure components and the eutectic mixture were determined from DSC studies. Excess Gibb's energy (G^E), excess enthalpy (H^E), and excess entropy (S^E) of mixing of pre-, post-, and the eutectic mixture were also calculated using activity coefficient data. Linear velocities of solidification of pure components and the eutectic mixture were determined at different undercooling rates. The values of the excess thermodynamic functions, linear velocity of crystallization, and ab initio calculations indicate the nonideal nature of the eutectic mixture in the melt. The anisotropic and instantaneous crystallizations of benzamide, *o*-chlorobenzoic acid, and the eutectic mixture were studied. The flexural strengths of the pure components and the eutectic mixture were also measured.

Introduction

A eutectic mixture is a composite material consisting of two or more solid phases, which are in equilibrium with a single liquid phase. The properties of such materials depend on the evolution of their microstructures.[1] Anisotropic growth is one of the most efficient techniques in the domain of solidification phenomena. Metallic composites are generally opaque in nature; hence, it is not possible to carry out visual observations on their growth front crystallizing from the melt. The problem of visual observation can be overcome by choosing transparent analogues of organic compounds as a model system. Studies have shown that there are organic compounds which solidify in the same way as metals. Eutectic solidification appears to be very simple, but the mechanism is quite complex. Despite extensive studies on solidification behavior of organic eutectic systems,[2−6] the mechanism is not fully explored. The nature of interactions may control the formation and properties of eutectic mixtures.[7,8] In the present paper, attempts have been made to understand the solidification behavior of benzamide (1) + *o*-chlorobenzoic acid (2) eutectic system.

Experimental

Materials. Benzamide (BM) and *o*-chlorobenzoic acid (*o*-CBA) are both from SD. Fine chemicals were purified by recrystallization from hot water. The melting points of purified samples were found to be (127.0 ± 0.1) °C, literature value was (126.2 ± 0.9) °C,[9] and (141.0 ± 0.1) °C, the literature value was (140.20 ± 0.15) °C,[9] respectively.

Phase Diagram Studies. The phase diagram of the BM + *o*-CBA system was studied by the thaw−melt method.[10] Accurate amounts of BM and *o*-CBA were weighed in glass tubes to make mixtures of different compositions. The glass tubes were sealed and heated in an oil bath at a temperature slightly higher than the melting temperatures of the components. The melts were shaken well and then chilled immediately in ice-cold water. To prepare homogeneous mixtures, the process of heating and chilling was repeated several times, and finally the tubes were broken. The solidified mass was crushed into fine powder. The melting points of the mixtures were determined with the help of a precision mercury thermometer which could read up to ± 0.1 °C. The melting points were plotted as a function of composition to obtain the phase diagram. The thaw points and the melting points of different mixtures with mean deviations are given in Table 1.

Table 1. Temperature−Composition Data of the Benzamide (1) + *o*-Chlorobenzoic Acid (2) Eutectic System

x_2	t_T[a]/°C	t_{fus}[b]/°C	t_u[c]/°C
1.0000	−	141.0 ± 0.1	137.6 ± 0.1
0.9516	71.9 ± 0.1	139.7 ± 0.1	134.0 ± 0.1
0.8636	71.8 ± 0.1	134.8 ± 0.1	127.0 ± 0.1
0.7647	71.2 ± 0.1	132.6 ± 0.1	115.7 ± 0.1
0.6338	72.6 ± 0.2	122.1 ± 0.1	95.2 ± 0.2
0.5000	71.9 ± 0.1	104.5 ± 0.1	72.5 ± 0.1
0.4559	−	72.8 ± 0.1	51.4 ± 0.1
0.4324	72.4 ± 0.1	81.2 ± 0.1	53.7 ± 0.1
0.3467	71.2 ± 0.1	108.0 ± 0.1	70.7 ± 0.1
0.2468	71.9 ± 0.1	114.7 ± 0.1	90.2 ± 0.1
0.1665	71.8 ± 0.1	118.4 ± 0.1	100.1 ± 0.1
0.0750	71.8 ± 0.1	123.8 ± 0.1	101.8 ± 0.1
0.0000	−	127.0 ± 0.1	112.0 ± 0.1

[a] t_T = Thaw melting temperature. [b] t_{fus}= Fusion temperature. [c] t_u = Undercooling temperature.

Undercooling Measurement. The undercooling measurements of various mixtures were carried out by the method described earlier.[10] Appropriate masses of the pure components and their mixtures of different compositions were taken in clean glass tubes, sealed, and immersed in a liquid paraffin oil bath maintained at a temperature slightly above their melting temperatures. After complete melting of the material, the temperature of the bath was slowly decreased (3 K·min^{-1}). The formation of the first crystallite was noticed by a magnifying glass, and each experiment was repeated at least five times. The temperature at which the first crystallite appeared was noted. The undercooling temperatures for different mixtures were

* Corresponding author. E-mail: ssdas2002@rediffmail.com.
† Part of the "Gerhard M. Schneider Festschrift".

10.1021/je800848u CCC: $40.75 © 2009 American Chemical Society
Published on Web 04/01/2009

recorded and are given in Table 1. The difference between the true melting temperature and this temperature gave the undercooling temperature.

Crystal Growth. The kinetics of solidification of BM, *o*-CBA, and the eutectic mixture were studied in a manner similar to that reported earlier.[11] Measurements were done in a U-shaped Pyrex glass tube (length 10 cm and diameter 0.8 cm) which was placed over a graduated scale. The tubes were filled with fine powders of the pure components and the eutectic mixture separately and placed in an oil thermostat maintained slightly above their melting temperatures. On complete melting of the sample, the temperatures were maintained at different undercooling, and a seed crystal of the same was introduced from one side of the tube to the melt. On adding the seed, crystal nucleation and crystallization started linearly in the tube. The time needed for a definite length of crystallization in the horizontal portion of the tube was recorded which gave the linear velocity of crystallization.

Determination of Enthalpies of Fusion. Values of enthalpy of fusion of benzamide, *o*-chlorobenzoic acid, and the eutectic mixture were determined from the DSC curves obtained with the help of a differential scanning calorimeter (METTLER STAR SW 900) in a nitrogen atmosphere at a heating rate of 5 $K \cdot min^{-1}$.

FT-IR Spectral Studies. FT-IR spectra of the pure components and the eutectic mixture were recorded on a BRUKER spectrometer in the wavelength range (4000 to 1500) cm^{-1} by using KBr pellets. The uncertainty in the instrument was $\pm$ 5 cm^{-1}.

Computational Studies. The molecular geometries of (a) benzamide and (b) *o*-chlorobenzoic acid in the gaseous phase have been optimized by using an ab initio (GAMESS with 6-21G* basis set) program.[12] This has been done by using Z-matrix, which is prepared with the help of bond length, bond angle, and dihedral angles of the molecules. The net charge and dipole components located at each of the atomic centers of these molecules have been computed by using the GAMESS program fitted with the 6-21G* basis set. The modified Rayleigh−Schrödinger second-order perturbation theory along with the multicentered−multipole expansion technique, as developed by Claverie and co-workers,[13−15] has been used to evaluate intermolecular interactions between the molecules.

Optimized molecular geometry, charge distribution, and atomic dipole components have been constructed using the 6-21G* basis set by using the GAMESS an ab initio program.[12] The total interaction energy (E_{tot}) between the molecules is expressed as[16]

$$E_{tot} = E_{el} + E_{pol} + E_{disp} + E_{rep} \quad (1)$$

where E_{el}, E_{pol}, E_{disp}, and E_{rep} represent electrostatic, polarization, dispersion, and repulsion energy components, respectively, and are discussed below.

Electrostatic Energy: According to the multicentered−multipole expansion method, the electrostatic energy term is expressed as

$$E_{el} = E_{qq} + E_{qmi} + E_{mimi} + ... \quad (2)$$

where E_{qq}, E_{qmi}, and E_{mimi}, etc. represent monopole−monopole, monopole−dipole, dipole−dipole, and interaction energy terms consisting of multipoles of higher orders, respectively. The electrostatic component arising due to higher-order multipole moments also exists, but only an evaluation of electrostatic energy up to the first three terms has been found suitable for most of the cases.[13−15]

Again, monopole−monopole energy is given by eq 3.

$$E_{qq} = C \sum_{i,j} \frac{q_i q_j}{r_{i,j}} \quad (3)$$

where q_i and q_j are monopoles at each of the atomic centers of the interacting molecules, while r_{ij} is the interatomic distance. The constant, C, is a conversion factor, approximately equal to 332, which expresses the energy in kilocalories per mole of the dimer.

The monopole−dipole energy is expressed as

$$E_{qmi} = C \sum_{i,j} q_i \vec{\mu}_j \cdot \frac{\vec{r}}{r^3} \quad (4)$$

while the dipole−dipole term is given by

$$E_{mimi} = C \sum_{i,j} \frac{1}{r^3}\left[\vec{\mu}_i \vec{\mu}_j - 3\left(\vec{\mu}_i \frac{\vec{r}}{r}\right)\left(\vec{\mu}_j \frac{\vec{r}}{r}\right)\right] \quad (5)$$

where μ_i and μ_j represent the atomic dipoles. The subscript of r has been removed without any change in its meaning, and other notations have the same meaning as in eq 3.

Polarization Energy: The polarization energy of a molecule, say *s*, is obtained as a sum of the polarization energies for the various bonds

$$E_{pol}^{(s)} = C\left(-\frac{1}{2}\right) \sum_{u}^{(s)} \varepsilon_u^{(s)} A_u^{(s)} \varepsilon_u^{(s)} \quad (6)$$

where

$$\varepsilon_u^{(s)} = \sum_{t \neq S} \sum_{\lambda}^{t} q_\lambda^{(t)} \vec{R}_{\lambda u} / R_{\lambda u}^3 \quad (7)$$

is the electric field created at bond u by all the surrounding molecules and A_u is the polarizability tensor of this bond. $\vec{R}_{\lambda u}$ is the vector joining the atom λ in the molecule (t) to the "center of polarizable charge" on the bond u of molecule (*s*).

Dispersion and Repulsion Energy. Dispersion and repulsion terms are calculated together using Kitaigorodskii[13−15] type formulas

$$E_{disp} + E_{rep} = \sum_{\lambda}^{(1)} \sum_{v}^{(2)} E(\lambda, v) \quad (8)$$

here

$$E(\lambda, \nu) = K_\lambda K_v \left(-\frac{A}{z^6} + Be^{-\gamma z}\right) \quad (9)$$

and

$$z = \frac{R_{\lambda v}}{R^0_{\lambda v}};\ R^0_{\lambda \nu} = \sqrt{(2R^{\mathrm{w}}_{\lambda})(2R^{\mathrm{w}}_{\nu})} \tag{10}$$

Here R^{w}_{λ} and R^{w}_{ν} are van der Waal's radii of atoms λ and v, respectively. The parameters A, B, and γ do not depend on the atomic species, but $R^0_{\lambda v}$ and the factors K_{λ} and K_{ν} depend on the atomic species involved.

The energy minimization has been carried out for both stacking and in-plane (side-to-side) interactions separately. One of the interacting molecules is kept fixed throughout the process, while both lateral and angular variations are introduced in the other in all respects relative to the fixed one. The first molecule has been assumed to be in the $x-y$ plane with the x-axis lying along the long molecular axis, while the origin is chosen approximately at the center of mass of the molecule. The second molecule has been translated initially along the z-axis (perpendicular to the molecular plane) and subsequently along the x and y axes. Variation of interaction energy with respect to rotation about the z-axis has been examined throughout the whole configurational space.

During energy optimization, both lateral and angular variations were introduced in one of the interacting molecules keeping the other molecule fixed and vice versa. Uncertainties up to 0.1 Å in translational (sliding) and 1° rotations have been achieved.[16]

Microstructural Studies. Small amounts of fine powders of BM, *o*-CBA, and the eutectic mixture were placed on separate glass slides. These slides were then placed in an oven maintained at a temperature slightly above their melting temperatures. Their melts were crystallized by moving separate glass coverslips over them in one direction. The microphotographs of the crystallized front were recorded with the help of a digital camera attached to an optical microscope (Olympus CHi20) at a magnification of 100×. The anisotropic as well as instantaneous growths of the materials were studied. For the study of instantaneous growth, small amounts of fine powders of the samples were kept on the glass slides and melted in an oven. The slides were then immediately placed over ice cubes, and glass coverslips were moved over them in one direction to initiate crystallization.

Flexural Strength Measurement. The samples were melted in a uniform cylindrical glass tube and then dipped vertically into an ice bath maintained at ≈0 °C, where solidification occurred. The solidified materials in the form of cylinders were then placed on the stand. A small container of known mass was allowed to hang in the middle of the cylindrical sample, where known weights were added to the container slowly until the cylindrical sample got ruptured. Moduli of rupture σ_{fs} of the materials were calculated with the help of the following eq 11.[17]

$$\sigma_{\mathrm{fs}} = \frac{F_{\mathrm{f}} L}{\pi R^3} \tag{11}$$

where F_{f} is the load at fracture; L is the distance between support points; and R is the specimen radius.

Results and Discussion

The solidus−liquidus equilibrium and spontaneous crystallization data of the BM (1) + *o*-CBA (2) system are graphically represented in Figure 1. The phase diagram curve indicates the formation of a eutectic mixture at $x_2 = 0.4559$ which melts at (72.8 ± 0.1) °C.

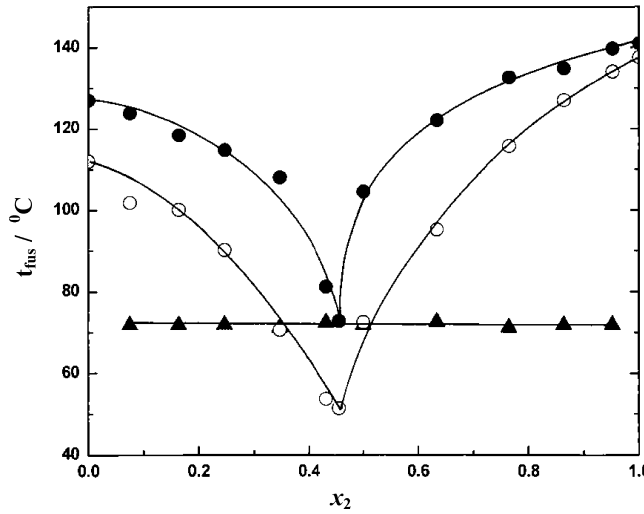

Figure 1. Phase diagram and undercooling of the benzamide (1) + *o*-chlorobenzoic acid (2) system: ▲, thaw melting temperature; ●, melting temperature; ○, undercooling temperature.

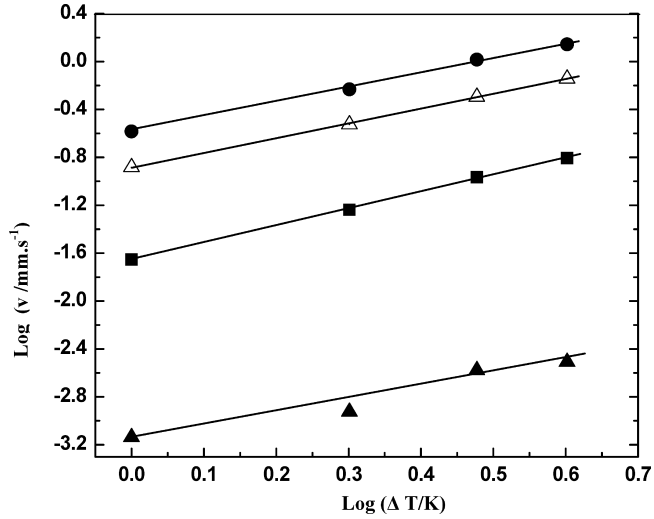

Figure 2. Linear velocity of solidification: ■, Benzamide; ●, *o*-Chlorobenzoic Acid; ▲, Eutectic (experimental); Δ, Eutectic (mixture law).

The anisotropic velocities of crystallization (v) of the eutectic mixture and the pure components measured at different undercoolings (ΔT) are shown in Figure 2 in the form of log v vs log ΔT plots. According to the Hillig−Turnbull[18] equation, the linear velocity of crystallization (v) and undercooling (ΔT) are related by eq 12.

$$v = k(\Delta T)^n \tag{12}$$

where k is the kinetic coefficient and n is a constant. The values of k and n in each case were determined from the intercepts and slopes of the straight lines (Figure 2). The experimental values of k and n are given in Table 2. These two crystallization parameters depend on the solidification behavior of materials. It is known that the experimental values of n close to 2 indicate the square relationship between the growth velocity and the undercooling. However, in the present system, the values of n are found to be lower than 2 (Table 2). This may be due to the difference between the bath temperature and the temperature of the growing interface. In the case of a eutectic mixture, the linear velocity of crystallization (v) was also calculated by using the mixture law, eq 13

$$v_e = x_1 v_1 + x_2 v_2 \quad (13)$$

where x_1 and x_2 are the mole fractions of components 1 and 2 and v_e, v_1, and v_2 are the linear velocities of crystallization of the eutectic mixture, component 1 and component 2, respectively. For the eutectic mixture, one also obtains a straight line when log v (as calculated from the mixture law) is plotted against log ΔT (Figure 2). From Figure 2, it is seen that the linear velocities of crystallization for the eutectic mixture at different undercoolings, calculated by the mixture law, are higher than the experimental values. This suggests the possibility of existence of some sort of weak interaction or molecular association between BM and *o*-CBA. Further, in the eutectic mixture, the experimental values of linear velocities of crystallization of the eutectic mixture are found to be lower than the linear velocities of crystallization of individual pure components. This could be explained on the basis of the mechanism as proposed by Wingard et al.[19] According to them, the growth begins with the nucleation of one of the phases having a high melting temperature. This growth continues until the surrounding liquid becomes rich in composition of the other component. As a result of increase in the concentration, the second component then also starts nucleating. In the case of the present eutectic, the solidification mechanism follows an alternate nucleation of the two components. Therefore, the eutectic system cannot be considered as a mechanical mixture of the two pure components.[20] The mode of crystallization, structure of eutectic melt, and the nature of interaction between the two components could be understood from the heat of fusion data of the pure components and the eutectic mixture. The enthalpies of fusion values experimentally determined from DSC studies and calculated by using the mixture law (eq 14) are given in Table 2.

Table 2. Crystallization Parameters and Enthalpy of Fusion Values for BM, *o*-CBA, and the Eutectic Mixture[a]

system	k/(mm·s^{-1}·K^{-1})	n	$\Delta_{fus}H$/(J·g^{-1})
benzamide	0.0223 ± 0.0004	1.41 ± 0.01	191.04
o-chlorobenzoic acid	0.2630 ± 0.0000	1.21 ± 0.01	175.86
eutectic mixture (experimental)	0.0008 ± 0.0001	1.04 ± 0.03	114.52
eutectic mixture (mixture law)	0.1303 ± 0.0015	1.23 ± 0.01	184.12

[a] ± denotes mean deviations in the values.

Table 3. Different Types of Interaction Energies (kJ·mol^{-1}) in the Benzamide (1) + *o*-Chlorobenzoic Acid (2) Eutectic System

energy terms	stacking	side-to-side (in plane)
E_{qq}	−2.88	−0.52
E_{qmi}	−82.98	−27.65
E_{mimi}	0.01	0.06
E_{el}	85.84	−28.11
E_{pol}	−1.37	−39.66
E_{disp}	−17.67	−34.52
E_{rep}	21.97	21.33
E_{tot}	−82.91	−45.26
separation/(Å)	13.82	26.79

$$(\Delta_{fus}H)_e = (x_1)_e(\Delta_{fus}H)_1 + (x_2)_e(\Delta_{fus}H)_2 \quad (14)$$

where $(\Delta_{fus}H)_1$ and $(\Delta_{fus}H)_2$ are the enthalpies of fusion of components 1 and 2, respectively. The experimentally determined value of the enthalpy of fusion (114.5 ± 0.9) J·g^{-1} for the eutectic mixture is much lower than the value (184.1 ± 0.8) J·g^{-1} as calculated from the mixture law. The lower enthalpy of fusion value indicates the existence of some interaction between the two components, viz. BM and *o*-CBA. Also, the enthalpy of fusion values of BM (191.04) J·g^{-1} or (23.1 ± 0.3) kJ·mol^{-1} and *o*-CBA (175.86) J·g^{-1} or (27.5 ± 0.2) kJ·mol^{-1} with mean deviations are higher than the value of the eutectic mixture. This may be explained on the basis of lower magnitude of interaction between the two components in the eutectic mixture in comparison to that which exists in the pure BM and *o*-CBA.

The deviation from ideal behavior of the eutectic can be expressed with the help of excess thermodynamic functions. The values of excess thermodynamic functions are also very important in the quantitative analysis of the nature of molecular interactions.[20] Thus, the excess functions such as G^E, H^E, and S^E were determined in a manner similar to that reported earlier[20,21] and discussed below.

The solidus−liquidus equilibrium boundary of the phase diagram of benzamide + *o*-chlorobenzoic acid system showing the formation of two eutectic mixtures can be predicted by the phase equilibrium relation[22] given by eq 15.

$$-\ln \gamma_i x_i = \frac{(\Delta H_f)_i}{R}\left[\frac{1}{T_e} - \frac{1}{T_i}\right] \quad (15)$$

where γ_i, x_i, $(\Delta H_f)_i$, and T_i are the activity coefficient, mole fraction, enthalpy of fusion, and melting temperature of the component i, respectively. R is a gas constant, and T_e is the melting temperature of the eutectic mixture. The excess Gibbs energy (G^E), excess entropy (S^E), and excess enthalpy (H^E) of mixing in the molten state were calculated by using eqs 16, 17, and 18 at the melting temperatures (T) of the mixtures.

Table 4. Activity Coefficient (ln γ_1, ln γ_2), Excess Gibbs Energy (G^E), Excess Enthalpy (H^E), and Excess Entropy (S^E) of the Benzamide (1) + *o*-Chlorobenzoic Acid (2) Eutectic System

x_2	T/K	ln γ_1	ln γ_2	$(\partial \ln \gamma_1)/(\partial T)$	$(\partial \ln \gamma_2)/(\partial T)$	G^E/(kJ·mol^{-1})	H^E/(kJ·mol^{-1})	S^E/(J·mol^{-1}·K^{-1})
0.9516	412.7	3.2424	0.0244	−0.0704	0.0150	0.62	−15.4	−38.9
0.8636	407.8	2.1253	0.0250	−0.0141	0.0151	1.06	−15.3	−40.2
0.7647	405.6	1.5429	0.1026	−0.0009	0.0146	1.49	−15.0	−40.7
0.6338	395.1	0.9183	0.0734	0.0064	0.0146	1.26	−15.0	−41.2
0.5000	377.5	0.2784	−0.0803	0.0111	0.0148	0.31	−15.4	−41.6
0.4559	345.8	−0.4821	−0.7915	0.0156	0.0185	−1.79	−16.8	−43.4
0.4324	354.2	−0.3335	−0.5122	0.0148	0.0167	−1.21	−16.3	−42.5
0.3467	381.0	0.0787	0.3664	0.0127	0.0107	0.57	−14.5	−39.6
0.2468	387.7	0.0626	0.8565	0.0129	0.0050	0.83	−13.7	−37.6
0.1665	391.4	0.0292	1.3309	0.0131	−0.0036	0.81	−13.1	−35.5
0.0750	396.8	0.0218	2.2435	0.0131	−0.0349	0.62	−12.5	−33.0

$$G^{E} = RT(x_1 \ln \gamma_1 + x_2 \ln \gamma_2) \quad (16)$$

$$H^{E} = -RT^2\left[x_1\frac{\partial \ln \gamma_1}{\partial T} + x_2\frac{\partial \ln \gamma_2}{\partial T}\right] \quad (17)$$

$$S^{E} = -R\left(x_1 \ln \gamma_1 + x_2 \ln \gamma_2 + x_1T\frac{\partial \ln \gamma_1}{\partial T} + x_2T\frac{\partial \ln \gamma_2}{\partial T}\right) \quad (18)$$

To determine $(\partial \ln \gamma_1)/(\partial T)$ and $(\partial \ln \gamma_2)/(\partial T)$, eq 15 is differentiated and rearranged as

$$x_i\frac{\partial \ln \gamma_i}{\partial T} = \frac{(\Delta H_f)_i}{RT^2}x_i - \frac{\partial x_i}{\partial T} \quad (19)$$

The liquidus curve in the phase diagram is reasonably straight in the region of eutectic composition. From this straight portion of the curve, the value of $(\partial x_i)/(\partial T)$ appearing in eq 19 may also be calculated. The calculated values of $(\partial x_i)/(\partial T)$, designated as a constant β, are related to mole fraction x_i by eq 20.

$$x_i = \alpha' + \beta T \quad (20)$$

where α' is another constant. By putting the value of β, mole fraction of component i, and the melting temperature (T) in eq 20, the value of α' can be calculated. Once the values of $(\partial x_i)/(\partial T)$ ($i = 1, 2$) are obtained, the values of $(\partial \ln \gamma_1)/(\partial T)$ and $(\partial \ln \gamma_2)/(\partial T)$ can be determined with the help of eq 19.

Thus, knowing the values of $(\partial \ln \gamma_1)/(\partial T)$ and $(\partial \ln \gamma_2)/(\partial T)$, the excess functions can be calculated from eqs 16, 17, and 18 and are given in Table 4, and their plots against mole fraction of *o*-CBA are shown in Figure 3. The results show that the values of G^E, H^E, and S^E are the minimum at the eutectic composition indicating maximum stability of the eutectic mixture.

The FT-IR spectra of BM, *o*-CBA, and their eutectic are shown in Figure 4. The results show that in the case of BM and *o*-CBA the peaks for the C═O group appear at a frequency of 1658 cm^{-1} and 1690 cm^{-1}, respectively, whereas in the case of a eutectic mixture the peak of the carbonyl group shows a slight shift and appears at a frequency of 1663 cm^{-1}. The shift in the stretching vibration of the C═O group indicates the presence of very weak H-bonding between the H-atom of the NH_2 group of BM and the O-atom of *o*-CBA.

Further intermolecular interactions between BM and *o*-CBA molecules have been evaluated during stacking and in-plane (side-by-side) configurations.[12] The optimized geometries of the molecules are shown in Figure 5. During stacking interactions, one of the molecules is kept fixed, while in the other molecule both positional as well as angular variations were simultaneously introduced and vice versa. The variation of total stacking energy with interplanar separation has been shown in Figure 6. As evident from this figure, a sharp and deep minimum is obtained at 3.3 Å with energy of −82.89 kJ·mol^{-1}. To obtain the minimum energy configuration, further calculations were carried out with accuracies of 0.1 Å in translation and 1° in rotation. The final optimum energy stacked configuration thus obtained (depicted in Figure 7a) bears an energy of −82.89 kJ·mol^{-1} at an interplanar separation of 3.3 Å between BM and *o*-CBA (Table 3). The in plane (side-by-side) interactions have also been evaluated by placing both of the molecules in one plane and

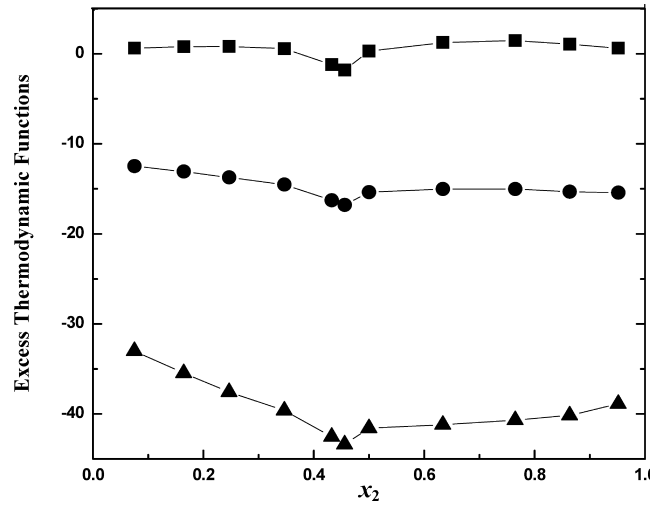

Figure 3. Excess thermodynamic functions: ■, excess Gibbs energy (G^E); ●, excess enthalpy (H^E); ▲, excess entropy (S^E).

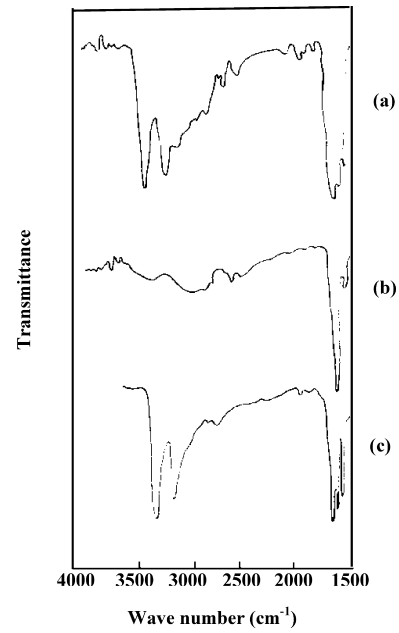

Figure 4. FT-IR spectra of (a) benzamide + *o*-chlorobenzoic acid eutectic, (b) *o*-chlorobenzoic acid, (c) benzamide.

introducing lateral and angular variations in one of the interacting molecules with respect to the other molecule keeping fixed and vice versa. The minimum energy configuration of BM and *o*-CBA during side-by-side interactions is shown in Figure 7b. The optimum distance between the centers of mass positions of the interacting molecules is 6.4 Å with energy of −45.26 kJ·mol^{-1} (Table 3).

As evident from Table 3, stacking attractions are higher than the in plane attractions between BM and *o*-CBA molecules. The largest contribution to the stability of the stacked and in plane configurations is derived from electrostatic and induced dipole-induced dipole (dispersion) type interactions, respectively. The relatively higher value of electrostatic attractions during stacking and nearly equal values of electrostatic and dispersion energies during in plane configurations demonstrate the strong possibility of the formation of hydrogen bonds between these molecules. These results indicate the existence of stable configurations of these molecules in the eutectic mixture.

The results obtained for the modulus of rupture indicate that the flexural strength of the components is practically negligible.

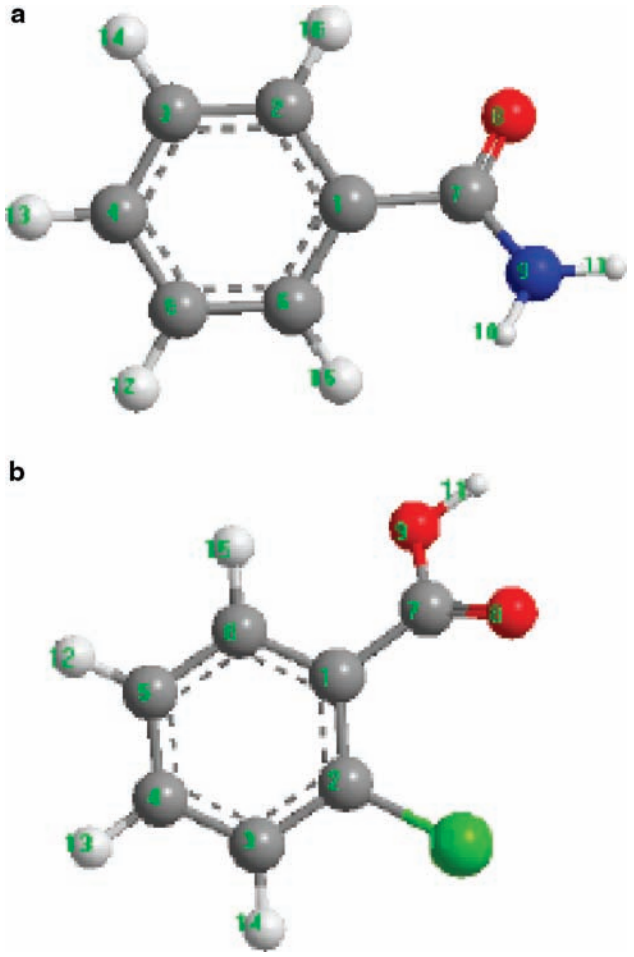

Figure 5. (a) Optimized geometry of benzamide. (b) Optimized geometry of *o*-chlorobenzoic acid.

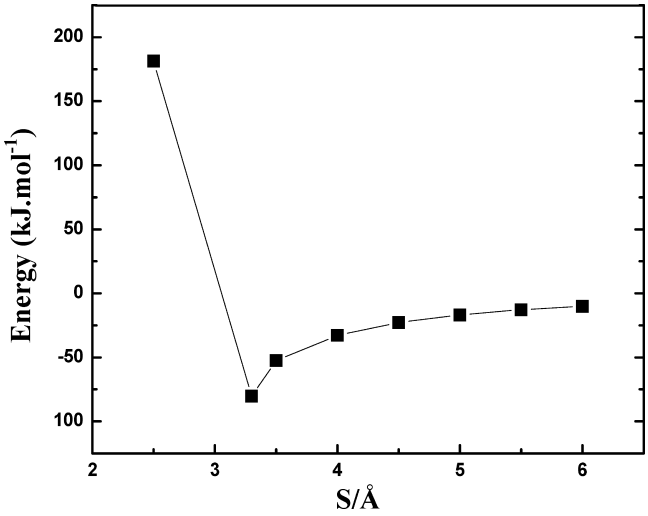

Figure 6. Potential energy diagram with respect to translation for the interaction of a pair of benzamide and *o*-chlorobenzoic acid molecules.

This may be due to breaking of the sample during isotropic growth. On the other hand, the flexural strength of the eutectic material was found to be (3.28 ± 0.03) MPa, which is much higher compared to those of the components. This may be explained on the basis of alignment of the components in the eutectic mixture in a definite fashion leading to a high flexural strength.

The study of microstructures (Figure 8) of the pure components and the eutectic mixture can explain the crystallization

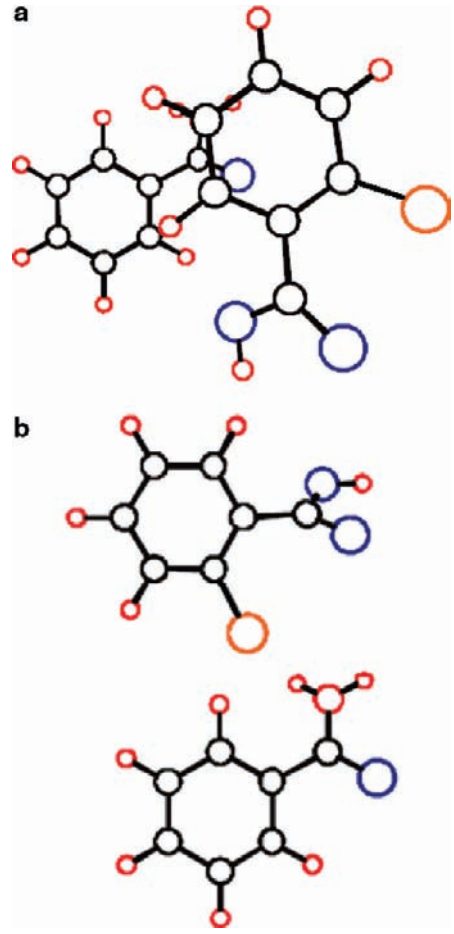

Figure 7. (a) Minimum energy configuration of benzamide and *o*-chlorobenzoic acid during stacking interactions with interplanar distance of 3.3 Å and energy of −82.89 kJ·mol^{-1}. (b) Minimum energy configuration of benzamide and *o*-chlorobenzoic acid during side-by-side interactions. The optimum distance between the centers of mass positions of the two molecules is 6.4 Å with energy −45.26 kJ·mol^{-1}.

behavior easily since various physical properties of the eutectic materials depend on their microstructures. In the case of anisotropic crystallization of BM, the microstructure appears to be an irregular broken lamellar type with thick lamellae (Figure 8a), whereas *o*-CBA when crystallized anisotropically gives lamellar-type structures with thin lamellae (Figure 8b) having very little spacing between the two lamellae. However, in the case of a eutectic mixture, a beautiful spherulitic-type structure (Figure 8c) is obtained. It may be noticed that the microstructures obtained on instantaneous crystallization are completely different from the anisotropic ones. The instantaneous microstructure of BM (Figure 8d) shows regular lamellar growth of rectangular shape. The instantaneous microstructure of *o*-CBA (Figure 8e) shows the formation of bamboo-type structures with small diameters growing in different directions from one point. On the other hand, the instantaneous microstructure of the BM−*o*-CBA eutectic (Figure 8f) is entirely different from the pure components. Here, in this case, the formation of small crystallites is very evident. It is reported that the formation of microstructures depends on various factors[4] such as (i) steady state heat flow, (ii) steady state diffusion, (iii) interface contact angles, (iv) kinetic equilibrium characteristics, and (v) nucleation characteristics of the two phases. Apart from the above conditions, the microstructure also depends on the defects such as (a) chemical inhomogeneity, (b) dislocations, (c) growth twins, (d) voids, and (e) stray crystals.

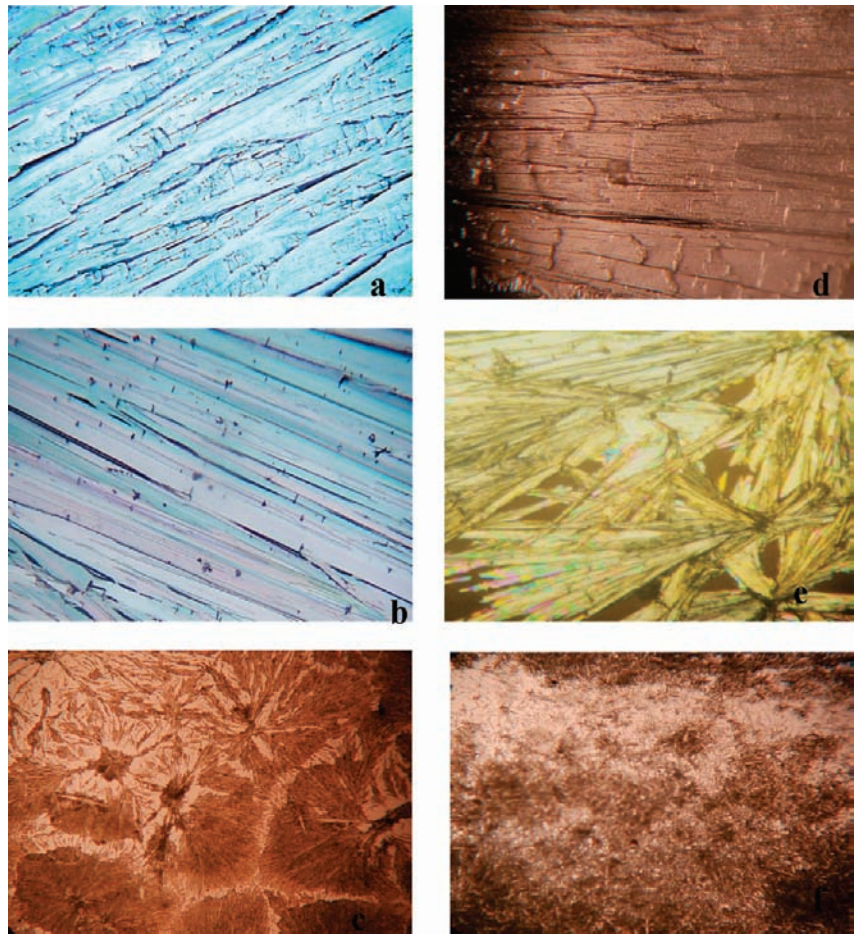

Figure 8. Microstructure of (a) pure BM (anisotropic growth), (b) pure *o*-CBA (anisotropic growth), (c) the BM + *o*-CBA eutectic mixture (anisotropic growth), (d) pure BM (instantaneous growth), (e) pure *o*-CBA (instantaneous growth), and (f) the BM + *o*-CBA eutectic mixture (instantaneous growth).

Therefore, it is difficult to predict the microstructure of the eutectic accurately. The growth morphology developed by a eutectic system is governed by the growth characteristics of individual constituent phases. Phases may solidify with nonfaceted or faceted interfaces. This solidification behavior is related to the nature of the solid/liquid interface and can be predicted from the entropy of fusion values. Jackson[23] was able to predict the structure of the solid/liquid interface of a material in contact with its liquid with the help of the roughness parameter by using eq 21.

$$\alpha = \xi \frac{\Delta_{fus}H}{RT_f} \qquad (21)$$

where ξ is the geometrical coefficient whose value lies between 0.5 and 1.0; $\Delta_{fus}H$ is the heat of fusion; T_f is the temperature; and R is the gas constant. The values of α for the two components and the eutectic mixture were calculated by putting the ξ value equal to 0.5 and 1.0, respectively. Jackson and Hunt[24] have reported that when $\alpha > 2$ the growth takes place with crystalline facets (i.e., the crystal develops a faceted morphology) and regular structures are not produced at all. In the present eutectic mixture, $\alpha > 2$, suggesting that the eutectic mixture possesses a faceted morphology with an irregular structure.

Conclusion

Phase diagram studies have shown that benzamide and *o*-chlorobenzoic acid form a simple eutectic mixture. Linear velocities of crystallization and excess thermodynamic functions have indicated that the eutectic is a nonideal mixture. IR spectral studies and ab initio calculations have shown the possibility of the formation of an H-bond between the molecules in the eutectic mixture. The flexural strength of the eutectic mixture is found to be higher than the components. On the basis of roughness parameters, it is predicted that the eutectic mixture possesses a faceted morphology with an irregular structure.

Literature Cited

(1) Elliott, R. *Eutectic Solidification Processing*; Butterworth: London, 1983.
(2) Chalmers, B. *Principles of Solidification*; John Wiley and Sons: New York, 1964.
(3) Elder, K. R.; Gunton, J. D.; Martin, G. Nonsothermal Eutectic Crysatillization. *Phys. Rev. E* **1996**, *54*, 6476–6484.
(4) Singh, N. B.; Das, S. S.; Singh, N. P.; Agrawal, T. Computer Simulation, Thermodynamic and Microstructural Studies on Benzamide-Benzoic acid Eutectic System. *J. Cryst. Growth* **2008**, *310*, 2878–2884.
(5) Gupta, R. K.; Singh, S. K.; Singh, R. A. Some Physicochemical Studies on Organic Eutectis. *J. Cryst. Growth* **2007**, *300*, 415–420.
(6) Witusiewicz, V. T.; Hecht, U.; Sturz, L.; Rex, S. Phase Eqillibria and Eutectic Growth in Ternary Eutectic System (D) Camphor-Neopentylgylcol-Succinonitrile. *J. Cryst. Growth* **2006**, *286*, 431–439.
(7) Gupta, R. K.; Singh, R. A. Thermochemical and Microstructural Studies on Binary Organic Eutectics and Complexes. *J. Cryst. Growth* **2004**, *26*, 340–347.
(8) Singh, N. B.; Giri, D. P.; Singh, N. P. Solid-Liquid Equillibria for p-Dichlorobenzene + p-Dibromobenzene and p-Dibromobenzene + Resorcinol. *J. Chem. Eng. Data* **1999**, *44*, 605–607.
(9) Zhang, Z.-Y.; Frenkel, M.; Marsh, K. N.; Wilhoit, R. C. *Enthaplies of Fusion and Transition of organic Compounds in Thermodynamic Properties of Organic Compounds and their Mixtures*; Marsh, K. N.,

Ed.; (Landolt-Börnstein-Index of organic compounds); Springer: 1995; Vol. 1V 8(A), ISBN 3-540-58854-x.
(10) Rastogi, R. P.; Verma, K. T. R. Solid-liquid Equilibrium in Solution of Non-Electrolyte. *J. Chem. Soc.* **1956**, 2097–2101.
(11) Rastogi, R. P.; Bassi, P. S. Mechanism on Eutectic Crystallization. *J. Phys. Chem.* **1964**, *68*, 2398–2406.
(12) Levine, I. N. *Quantum Chemistry*; Pearson Prentice Hall: 2006, 551.
(13) Claverie, P. *Intermolecular interaction: From Diatomics to Biopolymer*; Pullman, B. , Ed.; John Wiley: New York, 1978; p 69.
(14) Rein, R. On Physical Properties and Interaction of Polyatomic Molecules: With Application of Molecular Recognition in Biology. *Adv. Quantum Chem.* **1973**, *7*, 335.
(15) Langlet, J.; Claverie, P.; Caron, F.; Boeuve, J. C. Interactions between Nucleic Acid Bases in Hydrogen Bonded and Stacked Configurations: The Role of the Molecular Charge Distributions. *Int. J. Quantum Chem.* **1981**, *20*, 299.
(16) Tiwari, S. N.; Mishra, M.; Shukla, R. Theoretical Study of Molecular Ordering in p- n-Hexyloxybenzylidene-p-Toluidine: A Nematic Liquid Crystal. *Ind. J. Pure Appl. Phys.* **2007**, *45*, 83–88.
(17) Callister, W. D., Jr. *Materials Science and Engineering An Introduction*, 6th ed.; John Wiley & Sons: Inc.: New York, 2005; p 412.
(18) Hillig, H. B.; Turnbull, D. Theory of Crystal Growth in Undercooled Pure Liquid. *J. Chem. Phys.* **1956**, *24*, 914–920.
(19) Wingard, W. C.; Majka, S.; Thall, B. M.; Chalmers, B. Eutectic solidification in Metals. *Can. J. Chem.* **1954**, *29*, 320–327.
(20) Sharma, B. L.; Kant, R.; Sharma, R.; Tondon, S. Devitations of Binary Organic Eutectic Melts Systems. *Mater. Chem. Phys.* **2003**, *82*, 216–224.
(21) Singh, N. B.; Das, S. S.; Gupta, P.; Dwivedi, M. K. Phase Equillibria and Solidification Behaviour in Vanillin-p-Anisidine System. *J. Cryst. Growth* **2008**, *311*, 118–122.
(22) Rastogi, R. P. Thermodynamics of Phase Equillibria and Phase Diagram. *J. Chem. Educ.* **1964**, *41*, 443–448.
(23) Jackson, K. A. *Liquid metals and Solidification*; ASM: Cleveland, OH, 1958.
(24) Hunt, J. D.; Jackson, K. A. Lamellar and Rod Eutectic Growth. *Trans. Metall. Soc. AIME* **1966**, *236*, 1129–1142.

Received for review November 12, 2008. Accepted March 5, 2009.

JE800848U